

Structural Chirality and Natural Optical Activity across the α -to- β Phase Transition in SiO_2 and AlPO_4 from first-principles

F. Gómez-Ortiz,^{1,*} A. Zabalo,¹ A. M. Glazer,² E. E. McCabe,³ A. H. Romero,⁴ and E. Bousquet^{1,†}

¹*Physique Théorique des Matériaux, QMAT, CESAM,
Université de Liège, B-4000 Sart-Tilman, Belgium*

²*Department of Physics, Oxford University, Parks Road, Oxford OX1 3PU, United Kingdom*

³*Department of Physics, Durham University, South Road, Durham, DH1 3LE, U. K.*

⁴*Department of Physics and Astronomy, West Virginia University, Morgantown, WV 26505-6315, USA*

(Dated: October 6, 2025)

Natural optical activity (NOA), the ability of a material to rotate the plane of polarized light, has traditionally been associated with structural chirality. However, this relationship has often been oversimplified, leading to conceptual misunderstandings, particularly when attempts are made to directly correlate structural handedness with optical rotatory power. In reality, the relationship between chirality and NOA is more nuanced: optical activity can arise in both chiral and achiral crystal structures, and the sign of the rotation cannot necessarily be inferred from the handedness of the space group. In this work, we conduct a first-principles investigation of natural optical activity in SiO_2 and AlPO_4 crystals, focusing on their enantiomorphic structural phase transition from high-symmetry hexagonal ($P6_422$ or $P6_222$) to low-symmetry trigonal ($P3_121$ or $P3_221$) space groups. This transition, driven by the condensation of a zone-center Γ_3 phonon mode, reverses the screw axis type given by the space group symbol while leaving the sign of the optical activity unchanged. By following the evolution of the structure and the optical response along the transition pathway, we clarify the microscopic origin of this behavior. We demonstrate that the sense of optical rotation is determined not by the nominal helicity of the screw axis given in the space group symbol, but by the atomic-scale helicity of the most polarizable atoms of the structure.

I. INTRODUCTION

Natural optical activity (NOA) was first observed in the early 19th century by Arago [1] and Biot [2] when they discovered that certain materials could rotate the plane of polarization of light. Because atomic theory and electromagnetic theory were still nascent, the microscopic cause of this rotation and its broader significance remained unclear at the time. Since then, there have been several attempts to give a microscopic explanation of how NOA emerges in certain materials. Many theories have been developed [3–7], either applying electromagnetic theory or relying on atomic polarizabilities, as described in Ref. [8]. Currently, NOA is understood as a formal representation of the initial spatial dispersion of the macroscopic permittivity tensor as described by first-order principles [9, 10]. Moreover, it has recently become computationally accessible through first-principles density functional perturbation theory in both molecular and solid states efficiently and conveniently [11].

Finally, from an experimental point of view, NOA manifests itself through optical rotation, which can be measured by the rotation angle of the orientation of the plane of polarization about the optical axis of linearly polarized light as it travels through certain materials [3, 12–16].

While it is a well-known fact that NOA is frequently linked with structural chirality, it is currently understood

that chirality is a sufficient, albeit not necessary, condition for NOA to occur, given that achiral materials can also display NOA characteristics. [13, 17, 18]. This historical association led to the widespread belief that the chirality of a material's space group directly determines the handedness of its optical rotation [19, 20]. Although this correlation may hold in many cases, it is more nuanced: the direction of optical rotation does not necessarily follow the handedness/helicity given in the space group symbol. [21, 22]

Measurements of optical activity are a common practice for organic chiral molecules (e.g., sugars or tartaric acid) and, although comparatively weaker, remain measurable in inorganic crystals such as low-quartz and berlinite [21]. Quartz-crystal (SiO_2) adopts a trigonal structure (enantiomorphic space groups, $P3_121$ or $P3_221$) at room temperature (“ α -quartz”) and transforms sharply to hexagonal “ β -quartz” (enantiomorphic space groups, $P6_422$ or $P6_222$ respectively) at 573 °C; both polymorphs are chiral despite being built from achiral SiO_4 tetrahedra. Berlinite (AlPO_4), the structural analogue of quartz, similarly undergoes an $\alpha \rightarrow \beta$ transition at approximately 586 °C, passing from trigonal $P3_121$ ($P3_221$) symmetry to hexagonal $P6_422$ ($P6_222$) without disrupting the network of corner-sharing tetrahedra [23–25]. In such transitions, the sense of the principal screw axis of the space group symbol reverses sign; however, the sense of the optical activity of the crystal remains unchanged [22, 26]. Initially, it might appear counterintuitive, but the direction of rotation for the helix composed of the most polarizable atoms (which is unchanged throughout the transition) actually determines the direc-

* Corresponding author: fgomez@uliege.be

† Corresponding author: eric.bousquet@uliege.be

tion of optical activity, as shown by Glazer and Stadnicka. [21]. This explains why the optical activity is preserved despite the reversal of the principal screw axis in these crystal structures.

In this work, we aim to carry out an in-depth first-principles investigation of this structural transition and, following the workflow presented in Ref. [27], we show that it can be associated with the progressive condensation of a zone-center Γ_3 phonon mode consistent with symmetry analysis of rotations of SiO_4 units [28]. By following the evolution of the crystal structure from the high-symmetry (HS) to the low-symmetry (LS) enantiomorphic phase, we track how both the screw axis and the natural optical activity evolve along the transition path, providing microscopic insight into the interplay between chirality, lattice dynamics, and optical rotation.

II. COMPUTATIONAL DETAILS

For all the calculations, we converged the structural data of the parent structure with the ABINIT code [29] (version 9.10.5) with the PBEsol exchange-correlation functional. We used the plane wave-pseudopotential approach with optimized norm-conserving pseudopotentials as taken from the PseudoDojo server (v.4) [30, 31] and an energy cutoff of 40 Hartrees. The k -mesh sampling employed for the calculations was $6 \times 6 \times 6$ for the structural relaxations as well as for the computation of the NOA. A value of 10^{-6} Ha/Bohr was employed on the forces to stop the structural relaxations and a value of 10^{-7} Ha was used for the electronic residual self-consistent cycle stop. Phonon calculations were computed through the density functional perturbation theory framework as implemented in ABINIT [29, 32].

For the calculation of the optical activity, we focus on the low-frequency limit of $\bar{\rho}(\omega) = \rho(\omega)/(\hbar\omega)^2$, which tends to a constant as $\omega \rightarrow 0$, where $\rho(\omega)$ is the rotatory power and \hbar the reduced Planck constant. For both SiO_2 and AlPO_4 , we assume that the incident light propagates along the optic axis, which is considered to be parallel to the z Cartesian direction. Under these conditions, $\bar{\rho}(0) \simeq \frac{\eta_{xyz}}{2(\hbar c)^2}$, where c is the speed of light and η_{xyz} is a component of the natural optical activity tensor in the zero frequency limit. While numerous methodologies and strategies for computing the NOA in solids exist [4, 5, 7, 33–35], this study utilizes the latest linear-response approach grounded in density-functional perturbation theory developed by Zabalo and Stengel [11] and incorporated into ABINIT.

III. RESULTS

A. Structural transition of SiO_2 and AlPO_4

Let us start by analyzing the high-symmetry phase of SiO_2 , which crystallizes in the enantiomorphic $P6_422$ (or

$P6_222$) space group. For simplicity, we restrict our analysis to the $P6_422$ structure, as the methodology for the other space group is analogous and yields identical conclusions.

This structure is characterized by a network of corner-linked SiO_4 tetrahedra, arranged about a principal screw axis aligned with the crystallographic c -axis as shown in Fig. 1. Noticeably, the crystallization process fixes the chirality into the $P6_422$ (or $P6_222$) space group and the associated properties.

Recently, an algorithm has been proposed to identify chiral displacive transitions from achiral to chiral space groups [27], following the works of Fava et al. [36] for K_3NiO_2 . Applying this workflow [27] to SiO_2 and AlPO_4 , we find that a displacive phase transition from an achiral to a chiral space group is not allowed by pseudosymmetry. In other words, this means that an achiral phase of SiO_2 or AlPO_4 cannot be built from their enantiomorphic crystal structure if one wants a continuous small-atom distortion pattern connecting the two.

However, this pseudosymmetry search predicts that the high symmetry $P6_422$ right-handed screw-axis structure can be linked to the low-symmetry $P3_121$ left-handed screw-axis structure [24, 25] through the Γ_3 irrep of the zone center [28, 37] (or similarly between the $P6_222$ and the $P3_221$ space groups). This means that those two space groups can form a low-symmetry/high-symmetry pairs for SiO_2 or AlPO_4 . This kind of spontaneous symmetry breaking is possible since a chiral irreducible representation (or order parameter) can be formally defined [38], so that a group-subgroup relationship between two phases with distinct chirality is physically possible [39].

From our DFT calculations, we confirm the presence of an unstable phonon mode at the Γ point in the $P6_422$ phase of SiO_2 , as referenced by [40]. By checking the corresponding phonon eigenvector symmetry, we found that it has the Γ_3 irrep, i.e. in agreement with the symmetry analysis which links the right-handed screw of the high-symmetry phase and the left-handed screw of the low-symmetry phase. Such a mode is neither Raman nor infrared active, i.e. it is silent as reported some times ago through hyper-Raman [41] or inelastic neutron scattering [42]. Hence, these results go in the direction of the displacive character of the transition [43], helping clarify previous discussions on its nature [44]. The calculated structural data of the converged $P6_422$ structure computed with a k -mesh of $6 \times 6 \times 6$ can be found in Table I. From our DFPT calculations, we found that the imaginary frequency of the Γ_3 mode has an amplitude of $61i \text{ cm}^{-1}$. The condensation and relaxation of the Γ_3 eigenvector gives an energy difference between the high and low temperature phases of $\Delta E = -60 \text{ meV}$ per 9 atoms within the unit cell.

A symmetry adapted mode analysis using the ISODISTORT software [45, 46] of our relaxed low-symmetry phase reveals that the distortion decomposes into Γ_1 and Γ_3 irreps where the amplitude of the Γ_1 mode is marginal

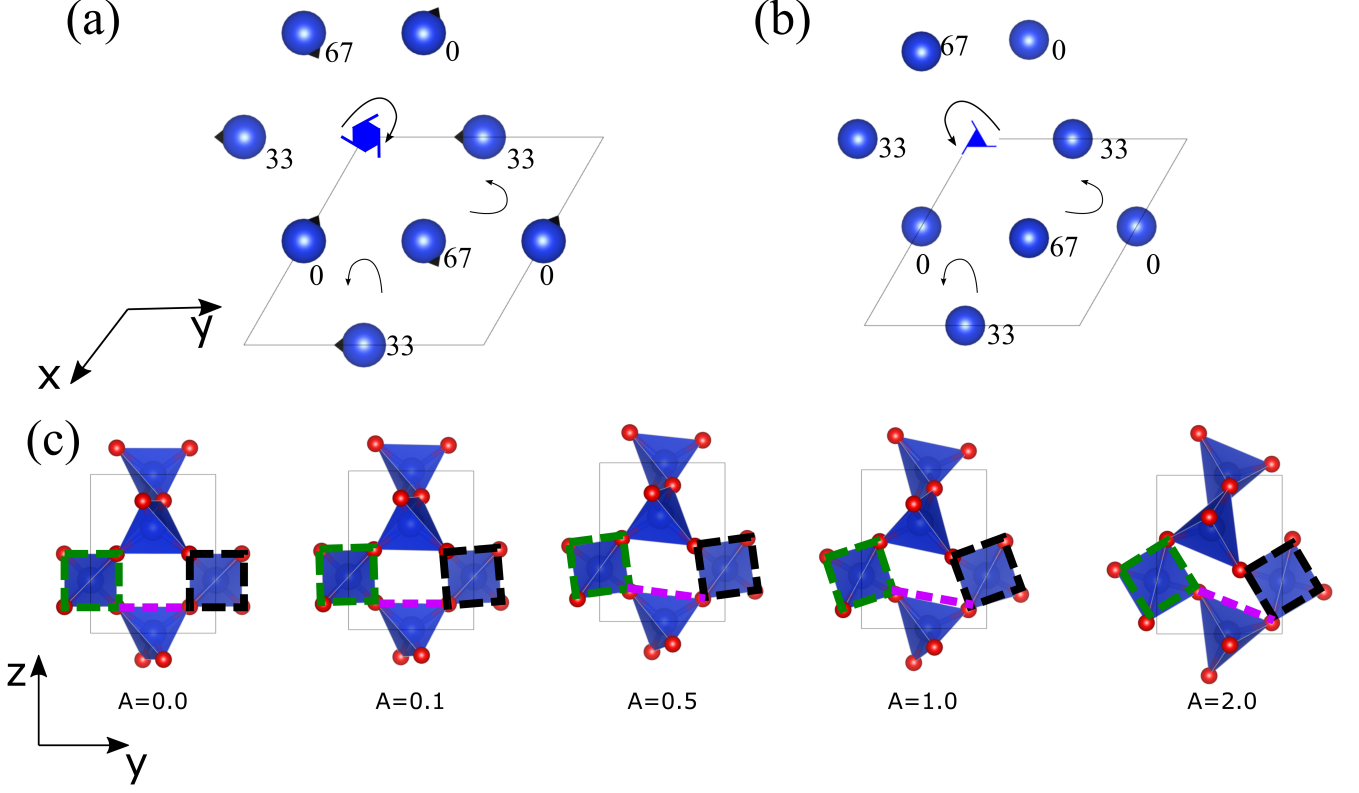


FIG. 1. Top views of the in-plane structural distortion in SiO_2 from the (a) $P6_422$ to the (b) $P3_121$ space groups with the movements of the Si atoms represented with black arrows in the atoms. Curved arrows are a guide to the eye indicating clockwise and counter-clockwise helix displayed by the Si atoms. (c) Side view illustrating the twisting of SiO_4 tetrahedra as a function of the Γ_3 mode amplitude. The amplitude $A = 1.0$ corresponds to the optimal distortion, yielding the maximum energy gain.

TABLE I. Relaxed DFT structural data (atom position along x , y and z directions) in reduced coordinates for the high symmetry phase ($P6_422$) of SiO_2 . The last three columns represent the atom displacements between the $P6_422$ and the $P3_122$ phases. The calculated cell parameters of the $P6_422$ structure are $a = b = 5.074$ Å and $c = 5.554$ Å and those of the $P3_122$ structure are $a = b = 4.951$ Å and $c = 5.441$ Å.

Atom	x	y	z	δ_x	δ_y	δ_z
Si (3a)	0.0000	0.5000	0.3333	0.0000	-0.0311	0.0000
O (6c)	0.2080	0.4160	0.8333	0.0606	-0.0038	-0.0484

(0.03 Å) with respect to the leading Γ_3 mode (1.00 Å) which drives the transition. The Γ_3 mode induces in-plane displacements of the Si atoms and both out-of-plane and in-plane displacements of the O atoms. The displacements are such that the SiO_4 tetrahedra rotate as fairly rigid units (and do not distort significantly), as illustrated in Figure 1(c). As shown in Fig. 1(a-b), the in-plane projection of the displacements induces a coordinated counter-clockwise and clockwise movement between the neighboring helical centers. This movement breaks the 6_4 -fold screw axis at the corners of the unit cells that transform into 3_1 centers while preserving the

3_1 -fold screw axis at the interior of the unit cell.

Moving now to the case of AlPO_4 crystal and when studying its $P6_422$ phase, we can observe a similar crystal structure to that of the $P6_222$ of SiO_2 [47, 48] with the exception that the c -axis is essentially doubled due to the ordering of Al + P over the atom sites (as discussed below). The crystal structure is shown in Fig. 2. The calculated structural data of the converged AlPO_4 $P6_422$ structure can be found in Table II. Similarly to the previous SiO_2 case, we also obtain an unstable phonon mode at the Γ point of the right-handed high-symmetry phase with an amplitude of $63i \text{ cm}^{-1}$ and the irrep Γ_3 [48]. This Γ_3 mode, hence, gives the link between the right-handed high-symmetry and the left-handed low-symmetry chiral phases, again similarly to the case of SiO_2 but with doubled cell along the z direction. The condensation and relaxation of the eigenvector of this Γ_3 unstable mode gives, in this case, an energy gain of $\Delta E = -155 \text{ meV}$ per 18 atoms unit cell, which is comparable to SiO_2 when normalized to the number of atoms. The relaxed structure we obtain is fully consistent with previous works [47, 49]. Similar conclusions to those drawn in the previous example can be reached by analyzing the distortion induced

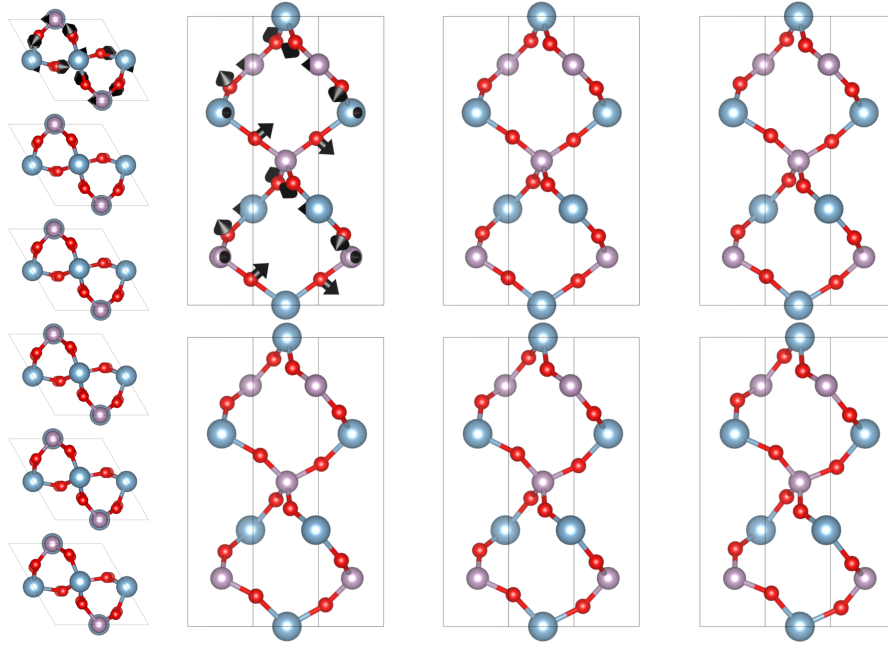


FIG. 2. Top (first left column figures) and side views of the progressive structural distortion in AlPO_4 from the $P6_422$ to the $P3_121$ space groups. The distortion amplitude increases from left to right and from top to bottom, in increments of 0.2, ranging from 0 (undistorted high symmetry phase) to 1 (relaxed low symmetry phase). Black arrows in the first panels indicate the directions of atomic displacements associated with the distortion. Red, blue and pink atoms correspond to O, Al and P respectively.

TABLE II. Relaxed DFT structural data (atom position along x , y and z directions) in reduced coordinates for the high symmetry phase ($P6_422$) of AlPO_4 . The last three columns represent the atom displacements between the $P6_422$ and the $P3_121$ phases. The relaxed cell parameters of the $P6_422$ phase are $a = b = 5.136\text{\AA}$, $c = 11.301\text{\AA}$ and those of the $P3_121$ phase are $a = b = 4.983\text{\AA}$, $c = 11.024\text{\AA}$.

Atom	x	y	z	δ_x	δ_y	δ_z
Al (3a)	0.5000	0.0000	0.3333	-0.0320	0.0000	0.0000
P (3b)	0.5000	0.0000	0.8333	-0.0318	0.0000	0.0000
O (6c)	0.1938	0.4201	0.0893	0.0616	-0.0049	0.0262
O (6c)	0.8062	0.5799	0.0893	0.0673	0.0040	-0.0243

by the Γ_3 mode, which causes in-plane displacements of the Al and P atoms and both in-plane and out-of-plane displacements of the O atoms as in the case of the quartz crystal. The symmetry adapted mode decomposition gives amplitudes of 0.08 \AA for the Γ_1 irrep and 1.57 \AA for the Γ_3 irrep.

Hence, we found with our calculations that both SiO_2 and AlPO_4 have an unstable phonon mode in their high-symmetry $P6_422$ (or, respectively, $P6_222$) chiral phase that drives the phase transition towards the lower temperature chiral structure $P3_121$ (or $P3_221$). We will now examine the connection between these phase transitions and their optical activity.

TABLE III. Evolution of the optical rotatory power $\bar{\rho}$ in $\frac{\text{deg}}{\text{mm}(\text{eV})^2}$ computed with first principles as a function of the normalized amplitude of the chiral distortion ξ from the $P6_422$ to the $P3_121$ phases of SiO_2 and AlPO_4 . The value at 0 and 1 corresponds to the optimal $P6_422$ and $P3_121$ phases.

ξ	$\bar{\rho}_{\text{SiO}_2}$	$\bar{\rho}_{\text{AlPO}_4}$
-1.0	5.4973	-4.3400
-0.8	5.8443	-4.7913
-0.6	6.2176	-5.2621
-0.5	6.4082	-5.4975
-0.4	6.5985	-5.7297
-0.2	6.9731	-6.1746
-0.1	7.1562	-6.3856
0.0	7.3364	-6.5884
0.1	7.1562	-6.3856
0.2	6.9731	-6.1746
0.4	6.5985	-5.7297
0.5	6.4082	-5.4975
0.6	6.2176	-5.2621
0.8	5.8443	-4.7913
1.0	5.4973	-4.3400

B. Evolution of the natural optical activity

To explore the microscopic origin of the optical activity in these systems, we now analyze the evolution of the NOA along the structural transition path from the high-symmetry to the low-symmetry enantiomorphic phases in both SiO_2 and AlPO_4 .

The results are summarized in Fig. 3 and Table III. The first interesting remark emerging from our calculations is the opposite sign of the NOA in the high-symmetry high-temperature $P6_422$ phases of SiO_2 and AlPO_4 , despite sharing the same enantiomorphic space group. Our first-principles calculations predict a positive rotatory power for the $P6_422$ and $P3_121$ phases of SiO_2 for light traveling along its optical axis, in agreement with Ref. [11] (despite the sign of the screw axis given in this space group symbol) and a negative rotatory power for light traveling along its optical axis for the $P6_422$ and $P3_121$ phases of AlPO_4 . The numerical values we obtained for SiO_2 are in good agreement with the values encountered in the literature [50] and the change of rotatory sign between SiO_2 and AlPO_4 is also consistent with a previous report by Glazer and Stadnicka [21]. This finding underscores a crucial concept: the sign of a crystal's natural optical activity links to its structural chirality, though it might not align with the helical handedness indicated by the space group symbol [21, 51]. This finding cautions against the common assumption that the sign of rotatory power unambiguously reflects the absolute sense of principal screw-axis [52] even in materials with similar space groups.

We can trace and explain the difference in rotatory power by examining the crystal structures of both materials. As mentioned in the previous section and now shown in Fig. 4, the atomic positions of AlPO_4 in its $P6_422$ setting are very similar to those of the SiO_2 crystal in its $P6_222$ setting. In fact, when we perform a computational experiment by substituting the Si atoms into the Al and P sites of the AlPO_4 structure, and calculate the optical activity, we obtain a rotatory power with the opposite sign to that of SiO_2 in its $P6_422$ phase and that closely resembles that found for AlPO_4 in its $P6_222$ phase. Furthermore, upon relaxing the atomic positions in this modified structure, the system naturally evolves into the $P6_222$ phase of SiO_2 although initially a $P6_422$ symmetry is detected by ABINIT. Although the one-to-one alternation of Al and P atoms and the non-equivalence of the O atoms induces a right-handed screw axis of the material as discussed in Ref. [21, 47], Fig. 4(d) shows that a non-symmetric left-handed helix similar to that observed in $P6_222$ SiO_2 is indeed present in the crystal. Although not perfectly symmetric, this helix of the most polarizable oxygen sites dominates the optical activity of these phases explaining its rotatory power [21, 51]. Moreover, the observation that substituting Si atoms at the Al and P sites does not significantly alter the rotatory power suggests that these atomic species contribute little to the optical activity, which mainly arises from the more polarizable oxygen atoms.

The second interesting observation is that the condensation of the chiral distortion decreases the value of the rotatory power in these types of transitions where the screw-axis type is reverted. Indeed, as shown in Fig. 3 we observe a linear decrease of the rotatory power as we condense the distortion. This can be explained by look-

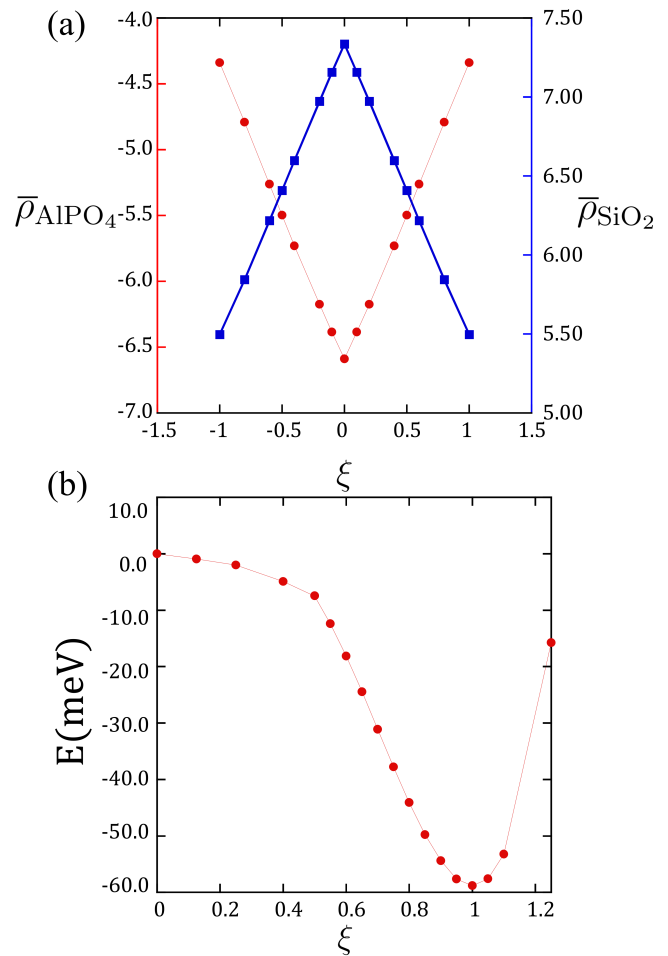


FIG. 3. (a) Evolution of the rotatory power (in units of $\frac{\text{deg}}{\text{mm} \cdot (\text{eV})^2}$) as a function of the condensation of the Γ_3 mode distortion connecting the $P6_422$ and $P3_121$ phases of AlPO_4 and SiO_2 . Red (left) and blue (right) axis correspond respectively to the rotatory power associated to the AlPO_4 and SiO_2 crystals. (b) Double well associated with the condensation of the unstable Γ_3 phonon mode eigendisplacement as calculated in SiO_2 . The crystal cell parameters are linearly interpolated between the two minima to model intermediate configurations.

ing at the distortions shown in Fig. 1 and Fig. 2 that tend to disrupt the helical arrangement of the O atoms. One might expect that further increasing the amplitude of the distortion could eventually revert the sign of the optical activity; however, our calculations show that, for instance, an amplitude 50% larger than the optimal value, recovers rotatory power values comparable to those of the undistorted high-symmetry phase. Moreover, this increase in distortion amplitude is accompanied by a significant increase in the Landau energy as shown in Fig. 3 (b), indicating that such configurations are physically inaccessible.

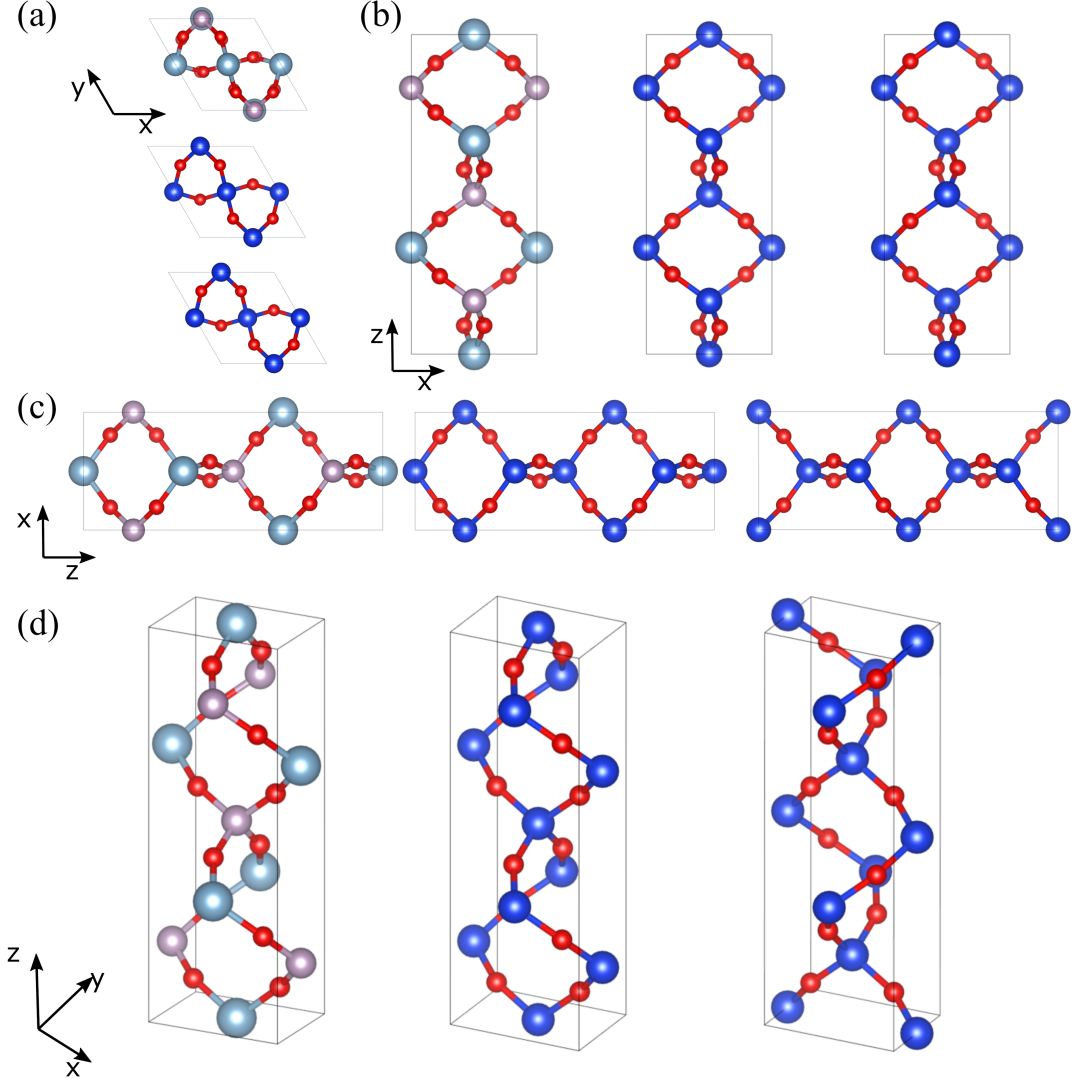


FIG. 4. Comparison of the crystal structures of $P6_422$ AlPO_4 , $P6_22$ SiO_2 and $P6_422$ SiO_2 ordered from top to bottom or left to right respectively in each case. The SiO_2 crystal structure has been duplicated along the c -axis for comparison purposes. (a-d) different views of the crystal structures as indicated by the corresponding cartesian axis. Dark blue, light blue, pink and red balls correspond to Si, Al, P and O atoms respectively.

IV. CONCLUSION

In this work, we performed an ab-initio analysis of the structural transitions and associated changes in the natural optical activity between the high-symmetry $P6_422$ ($P6_22$) and low-symmetry $P3_121$ ($P3_221$) phases of SiO_2 and AlPO_4 . Our first-principles calculations show that both materials undergo a displacive phase transition driven by the softening of a phonon mode at the zone center with Γ_3 symmetry. This mode induces a chiral distortion that reverses the sign of the principal screw-axis of the crystal high-symmetry space group.

Despite this reversal, the sense of the natural optical activity of the materials is preserved throughout the transition. AlPO_4 and SiO_2 therefore provide a useful

illustration of the principle that it is the helicity of the most polarizable atoms in a structure that determines the sign of its natural optical activity [21, 51]. Upon cooling through its $\beta - \alpha$ phase transition, the screw-sense of the imperfectly symmetric helix of oxygen sites is not changed (although this is not obvious from the space group symmetries of the α and β phases where the helix handedness given by the space group symbol is reversed), preserving therefore the optical activity of the system.

Interestingly, the closely related structures of AlPO_4 and SiO_2 also highlights the role of the most polarizable oxide ions. The AlPO_4 and SiO_2 structures differ due to the ordering of Al and P sites in AlPO_4 which doubles the c axis of the unit cell. As a result, the space groups of

the higher symmetry phases are reversed (high temperature AlPO_4 of $P6_422$ symmetry has atom sites, including those of the polarizable oxygens, close to those of SiO_2 of $P6_222$ symmetry). This means that the optical activity sign of $P6_422$ AlPO_4 is the same as that of $P6_222$ SiO_2 .

Furthermore, our analysis of the chiral distortion pathway indicates a linear decrease in the magnitude of the rotatory power as the Γ_3 mode progresses from the high-symmetry to the low-symmetry phase. This trend suggests that the symmetry-lowering introduced by the distortion reduces the helicity of the structure (as shown in Figure 3). Our results highlight the intricate relationship between structural chirality and optical activity in chiral crystals and caution against simplistic interpretations based solely on space group symmetry.

ACKNOWLEDGMENTS

F.G.O. acknowledges financial support from MSCA-PF 101148906 funded by the European Union and the Fonds de la Recherche Scientifique (FNRS) through the FNRS-CR 1.B.227.25F grant. F.G.-O. and E.B. acknowledge the Fonds de la Recherche Scientifique (FNRS) for financial support, the PDR project CHRYSALID No.40003544 and the Consortium des Équipements de Calcul Intensif (CÉCI), funded by the F.R.S.-FNRS under Grant No. 2.5020.11 as well as computational resources made available on Lucia, the Tier-1 supercomputer of the Walloon Region, infrastructure funded by the Walloon Region under the grant agreement No. 1910247. F.G.-O. and E. B. also acknowledge support from the European Union's Horizon 2020 research and innovation program under Grant Agreement No. 964931 (TSAR). We also recognize the support of the West Virginia High Education Policy Commission under the call Research Challenge Grand Program 2022, Award RCG 23-007 and NASA EPSCoR Award 80NSSC22M0173

-
- [1] F. Arago, Mémoire sur la polarisation colorée, Œuvres complètes de François Arago (1811).
 - [2] J. B. Biot, Sur de nouveaux rapports qui existent entre la réflexion et la polarisation de la lumière des corps cristallisés, Mem. Cl. Sci. Math. Phys. Inst. **13**, 1 (1812).
 - [3] E. U. Condon, Theories of optical rotatory power, *Rev. Mod. Phys.* **9**, 432 (1937).
 - [4] K. Natori, Band theory of the optical activity of crystals, *J. Phys. Soc. Jpn.* **39**, 1013 (1975).
 - [5] H. Zhong, Z. H. Levine, D. C. Allan, and J. W. Wilkins, Band-theoretic calculations of the optical-activity tensor of α -quartz and trigonal Se, *Phys. Rev. B* **48**, 1384 (1993).
 - [6] L. D. Barron, *Molecular Light Scattering and Optical Activity* (Cambridge University Press, Cambridge, England, 2009).
 - [7] Óscar Pozo Ocaña and I. Souza, Multipole theory of optical spatial dispersion in crystals, *SciPost Phys.* **14**, 118 (2023).
 - [8] V. A. Kizel', Optical activity and dissymmetry in living systems, *Phys. Usp.* **23**, 277 (1980).
 - [9] L. D. Landau and E. M. Lifshits, *Electrodynamics of Continuous Media. Volume 8 : Course of Theoretical Physics*, Second edition ed. (Pergamon, 1984).
 - [10] V. M. Agranovich and V. Ginzburg, *Crystal optics with spatial dispersion, and excitons* (Springer-Verlag, New York, 1984).
 - [11] A. Zabalo and M. Stengel, Natural optical activity from density-functional perturbation theory, *Phys. Rev. Lett.* **131**, 086902 (2023).
 - [12] J. Jerphagnon and D. S. Chemla, Optical activity of crystals, *J. Chem. Phys.* **65**, 1522 (1976).
 - [13] E. Bousquet, M. Fava, Z. Romestan, F. Gómez-Ortiz, E. E. McCabe, and A. H. Romero, Structural chirality and related properties in periodic inorganic solids: review and perspectives, *Journal of Physics: Condensed Matter* **37**, 163004 (2025).
 - [14] K. C. Nomura, Optical activity in tellurium, *Phys. Rev. Lett.* **5**, 500 (1960).
 - [15] S. Ades and C. H. Champness, Optical activity of tellurium to 20 μm , *J. Opt. Soc. Am.* **65**, 217 (1975).
 - [16] H. Iwasaki, K. Sugii, N. Niizeki, and H. Toyoda, Switching of optical rotatory power in ferroelectric $5\text{PbO } 3\text{GeO}_2$ single crystal, *Ferroelectrics* **3**, 157 (1972).
 - [17] P. S. Halasyamani and K. R. Poeppelmeier, Noncentrosymmetric oxides, *Chemistry of Materials* **10**, 2753 (1998).
 - [18] G. H. Fecher, J. Kübler, and C. Felser, Chirality in the solid state: Chiral crystal structures in chiral and achiral space groups, *Materials* **15**, 10.3390/ma15175812 (2022).
 - [19] W. A. Wooster, Physical properties and atomic arrangements in crystals, *Reports on Progress in Physics* **16**, 62 (1953).
 - [20] F. Gómez-Ortiz, M. Fava, E. E. McCabe, A. H. Romero, and E. Bousquet, Structural chirality measurements and computation of handedness in periodic solids, *Phys. Rev. B* **110**, 174112 (2024).
 - [21] A. M. Glazer and K. Stadnicka, On the origin of optical activity in crystal structures, *Journal of Applied Crystallography* **19**, 108 (1986).
 - [22] A. M. Glazer, Confusion over the description of the quartz structure yet again, *Journal of Applied Crystallography* **51**, 915 (2018).
 - [23] H. N. Ng and C. Calvo, X-ray study of the α - β transformation of berlinite (AlPO_4), *Canadian Journal of Physics* **54**, 638 (1976).
 - [24] S. M. Shapiro, D. C. O'Shea, and H. Z. Cummins, Raman scattering study of the alpha-beta phase transition in quartz, *Phys. Rev. Lett.* **19**, 361 (1967).
 - [25] H. Grimm and B. Dorner, On the mechanism of the α - β phase transformation of quartz, *Journal of Physics and Chemistry of Solids* **36**, 407 (1975).

- [26] J. D. H. Donnay and Y. Le Page, The vicissitudes of the low-quartz crystal setting or the pitfalls of enantiomorphism, *Acta Crystallographica Section A* **34**, 584 (1978).
- [27] F. Gómez-Ortiz, A. H. Romero, and E. Bousquet, *Pathways to crystal chirality an algorithm to identify new displacive chiral phase transitions* (2025), [arXiv:2503.13076 \[cond-mat.mtrl-sci\]](https://arxiv.org/abs/2503.13076).
- [28] B. Campbell, C. J. Howard, T. B. Averett, T. A. Whittle, S. Schmid, S. Machlus, C. Yost, and H. T. Stokes, An algebraic approach to cooperative rotations in networks of interconnected rigid units, *Acta Crystallographica Section A* **74**, 408 (2018).
- [29] X. Gonze, B. Amadon, G. Antonius, F. Arnardi, L. Baguet, J.-M. Beuken, J. Bieder, F. Bottin, J. Bouchet, E. Bousquet, N. Brouwer, F. Bruneval, G. Brunin, T. Cavignac, J.-B. Charraud, W. Chen, M. Côté, S. Cottenier, J. Denier, G. Geneste, P. Ghosez, M. Giantomassi, Y. Gillet, O. Gingras, D. R. Hamann, G. Hautier, X. He, N. Helbig, N. Holzwarth, Y. Jia, F. Jollet, W. Lafargue-Dit-Hauret, K. Lejaeghere, M. A. Marques, A. Martin, C. Martins, H. P. Miranda, F. Naccarato, K. Persson, G. Petretto, V. Planes, Y. Pouillon, S. Prokhorenko, F. Ricci, G.-M. Rignanese, A. H. Romero, M. M. Schmitt, M. Torrent, M. J. van Setten, B. Van Troeye, M. J. Verstraete, G. Zerah, and J. W. Zwanziger, The Abinitproject: Impact, environment and recent developments, *Computer Physics Communications* **248**, 107042 (2020).
- [30] D. Hamann, Optimized norm-conserving vanderbilt pseudopotentials, *Physical Review B* **88**, 085117 (2013).
- [31] M. J. Van Setten, M. Giantomassi, E. Bousquet, M. J. Verstraete, D. R. Hamann, X. Gonze, and G.-M. Rignanese, The pseudodojo: Training and grading a 85 element optimized norm-conserving pseudopotential table, *Computer Physics Communications* **226**, 39 (2018).
- [32] X. Gonze and C. Lee, Dynamical matrices, Born effective charges, dielectric permittivity tensors, and interatomic force constants from density-functional perturbation theory, *Physical Review B* **55**, 10355 (1997).
- [33] A. Malashevich and I. Souza, Band theory of spatial dispersion in magnetoelectrics, *Phys. Rev. B* **82**, 245118 (2010).
- [34] X. Wang and Y. Yan, Optical activity of solids from first principles, *Phys. Rev. B* **107**, 045201 (2023).
- [35] A. Urru, I. Souza, O. P. Ocaña, S. S. Tsirkin, and D. Vanderbilt, Optical spatial dispersion via wannier interpolation, *Phys. Rev. B* **112**, 045201 (2025).
- [36] M. Fava, E. McCabe, A. H. Romero, and E. Bousquet, A phonon-driven mechanism for an emergent and reversible chirality in crystals (2024), [arXiv:2405.12696 \[cond-mat.mtrl-sci\]](https://arxiv.org/abs/2405.12696).
- [37] S. M. Antao, Quartz: structural and thermodynamic analyses across the $\alpha \leftrightarrow \beta$ transition with origin of negative thermal expansion (NTE) in β quartz and calcite, *Acta Crystallographica Section B* **72**, 249 (2016).
- [38] J. Hlinka, Eight types of symmetrically distinct vectorlike physical quantities, *Phys. Rev. Lett.* **113**, 165502 (2014).
- [39] K. C. Erb and J. Hlinka, Symmetry guide to chiroaxial transitions, *Phase Transitions* **91**, 953 (2018).
- [40] C. V. Raman and T. M. K. Nedungadi, The α - β transformation of quartz, *Nature* **145**, 147 (1940).
- [41] Y. Tezuka, S. Shin, and M. Ishigame, Observation of the silent soft phonon in β -quartz by means of hyper-raman scattering, *Phys. Rev. Lett.* **66**, 2356 (1991).
- [42] J. D. Axe and G. Shirane, Study of the $\alpha - \beta$ quartz phase transformation by inelastic neutron scattering, *Phys. Rev. B* **1**, 342 (1970).
- [43] N. Choudhury and S. L. Chaplot, Ab initio studies of phonon softening and high-pressure phase transitions of α -quartz SiO_2 , *Phys. Rev. B* **73**, 094304 (2006).
- [44] G. Dolino, J.-P. Bachheimer, F. Gervais, and A. F. Wright, La transition α - β du quartz; le point sur quelques problèmes actuels: Transition ordre-désordre ou displacive, comportement thermodynamique, *Bulletin de Minéralogie* **106**, 267 (1983).
- [45] H. T. Stokes, D. M. Hatch, and B. J. Campbell, ISODIS-TORT, ISOTROPY software suite, iso.byu.edu.
- [46] B. J. Campbell, H. T. Stokes, D. E. Tanner, and D. M. Hatch, *ISODISPLACE*: a web-based tool for exploring structural distortions, *J. Appl. Crystallogr.* **39**, 607 (2006).
- [47] D. Schwarzenbach, Verfeinerung der struktur der tiefquarz-modifikation von alpo_4 , *Zeitschrift für Kristallographie - Crystalline Materials* **123**, 161 (1966).
- [48] Y. Muraoka and K. Kihara, The temperature dependence of the crystal structure of berlinite, a quartz-type form of AlPO_4 , *Physics and Chemistry of Minerals* **24**, 243 (1997).
- [49] N. Thong and D. Schwarzenbach, The use of electric field gradient calculations in charge density refinements. II. Charge density refinement of the low-quartz structure of aluminum phosphate, *Acta Crystallographica Section A* **35**, 658 (1979).
- [50] L. Jönsson, Z. H. Levine, and J. W. Wilkins, Large local-field corrections in optical rotatory power of quartz and selenium, *Phys. Rev. Lett.* **76**, 1372 (1996).
- [51] A. M. Glazer and K. Stadnicka, On the use of the term ‘absolute’ in crystallography, *Acta Crystallographica Section A* **45**, 234 (1989).
- [52] Y. Tanaka, T. Kojima, Y. Takata, A. Chainani, S. W. Lovesey, K. S. Knight, T. Takeuchi, M. Oura, Y. Senba, H. Ohashi, and S. Shin, Determination of structural chirality of berlinite and quartz using resonant x-ray diffraction with circularly polarized x-rays, *Phys. Rev. B* **81**, 144104 (2010).